2014

Deformation Mechanisms in the Metasedimentary Rocks Within the Kellyland Fault Zone, Washington County, Maine

Morgan E. Monz
Colby College

DEFORMATION MECHANISMS IN THE METASEDIMENTARY ROCKS WITHIN THE KELLYLAND FAULT ZONE, WASHINGTON COUNTY, MAINE

Morgan Monz ‘14

A Thesis

Submitted to the Faculty of the Geology Department of Colby College in Fulfillment of the Requirements for Honors in Geology

Waterville, ME

May 2014

DEFORMATION MECHANISMS IN THE METASEDIMENTARY ROCKS WITHIN THE KELLYLAND FAULT ZONE, WASHINGTON COUNTY, MAINE

Except where the reference is made to the work of others, the work described in this thesis is my own or was done in collaboration with my advisory committee.

Morgan E. Monz '14

Certificate of Approval:

Dr. Walter A. Sullivan
Assistant Professor
Department of Geology

Dr. Robert E. Nelson
Professor
Department of Geology

Dr. Robert A. Gastaldo
Whipple-Coddington Professor
Department of Geology

Abstract

This study focuses on a high-strain, strike-slip shear zone that juxtaposed metasedimentary rocks and a homogenous granite near the brittle-ductile transition, at a depth of 15-20 km. The metasedimentary rocks of the Flume Ridge Formation (FRF) exhibit a progressive deformation gradient of phase mixing and increasing fabric intensity across strike, northwest-to-southeast, approaching the center of the shear zone. Deformation mechanisms were controlled by metasomatic reactions in a fluid-rich fault zone. During deformation, biotite and potassium feldspar in the metasedimentary rocks reacted to form phengite—a much weaker phase. The nucleation and growth of weak phases, combined with phase mixing, decreased the shear strength of the rock. Phengite also branches at sharp angles to the foliation, and occurs preferentially along grain boundaries and dilatational sites indicating that these very fine-grained rocks deformed by granular flow. Hence, the cyclic process of solution precipitation and chemical alteration with granular flow governed the rheology of the metasedimentary rocks. Specific case studies such as this one can help to understand deformation mechanisms occurring in active fault zones at depth.

Acknowledgements

I would like to thank Dr. Walter (Bill) Sullivan for this research opportunity and his guidance and expertise throughout this process for the past two years. He has helped me learn more than I ever thought I could take away from a college experience, and I am immensely grateful. I would also like to thank Dr. Robert Gastaldo, Dr. Robert Nelson, and Dr. Bruce Rueger for the valuable input and critiques they have given me over this process, and for the valuable support. I would like to thank Dr. Don Allen for the time and energy he spent helping me learn how to work with the SEM, and Justin Sperry for all of his help in the field. I would like to thank Chuck Jones for fixing anything and everything that I broke throughout this process, putting up with all of my trouble making, and for his immense moral support. This project would not have been possible without all of his help. I would like to thank Ariana Boyd, Alice Ridky and Abby Pearson for keeping me marginally sane throughout this process. Finally, I would like to thank my parents, Betty and Dave Monz for their support and inspiration.

Table of Contents

1. Introduction

Deformation at active plate boundaries is primarily accommodated by faults and ductile shear zones. The continental lithosphere is thought to consist of a weak lower crust that lies between a strong upper crust and the uppermost mantle (Chen and Molnar, 1983; Thatcher and Polltz, 2008). Some authors have argued that post-seismic data indicate a strong upper mantle with high strain rates immediately following a large earthquake; however, as effective viscosity decreases with time and strain rates drop, mantle strength diminishes over geologic time scales (Jackson, 2002; Thatcher and Polltz, 2008). If this interpretation is correct, the brittle-ductile transition zone in the upper crust is the strongest part of the continental lithosphere, and, therefore, controls plate-tectonic processes (Jackson, 2002; Thatcher and Polltz, 2008).

Near the brittle-ductile transition, deformation is typically localized in shear zones as a result of strain weakening (Sibson, 1977; Kirby, 1985; Platt and Behr, 2011). There are three major mechanisms by which strain weakening can occur: 1) grain-size reduction by brittle fracturing or dynamic recrystallization (e.g., Tullis and Yund, 1985; Handy et al., 2007; Platt and Behr, 2011; Sullivan et al., 2013), 2) interconnection of weak phases or zones (e.g., Holyoke and Tullis, 2006), and 3) chemical alteration (e.g., O'Hara, 1988; Hippertt and Hongn, 1998). These mechanisms allow the concentration of strain in discrete shear zones, and control crustal strength over time (Sibson, 1977; Kirby, 1985; Plat and Behr, 2011; Montesi, 2013). The complex relationships between these strain-weakening mechanisms and their various roles are dependent on different conditions in evolving shear zones that are not well understood and difficult to accurately simulate in a laboratory (Sibson, 1977; Thatcher and Polltz, 2008; Sullivan et al., 2013). Therefore, to understand these mechanisms fully, more detailed case studies of naturally deformed rocks are necessary.

The southern half of the Kellyland fault zone (KFZ) in Washington County, Maine, is an ideal place to study strain weakening in low-grade metasedimentary rocks. Here, the KFZ juxtaposes the eastern lobe of the homogeneous Deblois Granite and the Flume Ridge Formation (FRF), which is a calcareous wacke interbedded with pelitic intervals (Figs. 1, 2) (Wang and Ludman, 2004; Wang 2007). Greenschist and subgreenschist-facies regional metamorphism of the FRF during the Middle to Late Silurian, coupled with brittle-ductile strain localization in the granite, indicate that this segment of the Norumbega Fault System (NFS) formed at shallow crustal levels near the brittle to ductile transition zone (Ludman, 1997; Sullivan et al., 2013).

Recently, Sullivan et. al. (2013) documented the deformation mechanisms that operated in the homogeneous granite on the southeast side of the shear zone in this area (Fig. 2). The deformed granite exhibits three distinct strain facies approaching the center of the shear zone: 1) foliated granite, 2) foliated granite cut by localized shear zones, and 3) a main ultramylonite domain (Sullivan et al., 2013). The formation of the ultramylonites and localized shear zones in the granite was catalyzed by a phase of brittle grain-size reduction (Sullivan et al., 2013). Neither domain experienced bulk chemical alteration or significant phase transitions during deformation, indicating a lack of fluid mobility in the granite rocks cut by the shear zone (Sullivan et al., 2013). However, carbonate-rich mylonites bearing sheet silicates, like those in the FRF cut by the KFZ, generally deform via complex interactions of granular flow and solution-transfer processes, which involve fluid flux during deformation (e.g., Herwegh and Jenni, 2000; Wintsch et al., 2005; Wallis et al., 2013). This study will compare and contrast the mechanisms of deformation in the metasedimentary rocks of the FRF and the homogeneous granite to further characterize deformation mechanisms that operated synchronously in different rock types in a shear zone near the brittle to ductile transition.

2. Background

2.1 Geologic Setting

The Norumbega Fault System (NFS) is a long-lived dextral strike-slip system that is comparable in extent to, if not larger than, the modern San Andreas fault system (Ludman and West, 1999; Wang and Ludman, 2004). Subparallel faults and shear zones that comprise the system can be traced throughout the northern Appalachian Mountains, and record a complex polyphase history of plate tectonic movement that is still debated (Goldstein and Hepburn, 1999; West and Roden-Tice, 2003). In eastern Maine, the NFS records both ductile and brittle deformation from the middle to late Paleozoic (Wang and Ludman, 2004). Here, the NFS is partitioned into three lower-greenschist-facies shear zones ranging from 0.5-5 km in width (Ludman and Gibbons, 1999; Wang and Ludman, 2004). From north to south, these are the Codyville fault zone, the Waite fault zone, and the Kellyland fault zone (Fig. 1) (Wang and Ludman, 2004). The KFZ records Neo-Acadian ductile and brittle deformation, and it juxtaposes the FRF and the eastern lobe of the Deblois granite in this area (Ludman and Gibbons, 1999; Ludman and Berry, 2003; Wang and Ludman, 2004; Sullivan et al., 2013).

2.2 The Flume Ridge Formation

The FRF consists of medium to thick beds of calcareous, fine- to medium-grained, homogeneous, quartzofeldspathic wacke and thinner pelitic interbeds of calcareous and non-calcareous siltstone (Wang, 2007). These beds were deposited in the migrating Avalon terrane foreland basin in the early Silurian (Bradley et al., 2000). During the Middle to Late Silurian, the FRF experienced chlorite-grade metamorphism and extensive, tight folding (Ludman, 1997; Wang and Ludman, 2004). The folds are disharmonic due to lithologic vaiation and increase in

intensity and amplitude approaching the Fredericton Fault in eastern New Brunswick, Canada (Park and Whitehead, 2003). The Silurian fold axial surfaces are upright to steeply inclined and fold axes are horizontal or plunge gently to the northeast and southwest (Park and Whitehead, 2003; Wang and Ludman, 2004).

2.3 The Deblois granite

The Deblois granite is the single largest intrusion in the Devonian intrusive suite of coastal Maine. It intruded the FRF during the Devonian, and it was cut by the KFZ shortly after it crystallized (Ludman et al., 1993; Wang and Ludman, 2004). U-Pb analyses of zircons from the undeformed granite yield an upper-intercept age of 383±14 Ma and a lower-intercept age of 87±150 Ma (Ludman and West, 1999). Large age uncertainties are due to low uranium content in the zircons, and low $^{206}Pb/^{204}Pb$ ratios. A more precise mean age was obtained from strongly foliated granite at the margin of the KFZ where $^{207}Pb/^{206}Pb$ ratios yielded an age of 384±5 Ma (Ludman and West, 1999). In the area of this study, the Deblois granite pluton is homogeneous and megacrystic to pegmatitic, and it has a primary mineral assemblage of microcline, quartz, oligoclase, biotite, and hornblende (Wang and Ludman, 2004; Wang, 2007; Sullivan et al., 2013). Approximately 20% of the microcline crystals in the granite exhibit Rapakivi overgrowths of plagioclase (Wang, 2007).

The KFZ created three distinct strain facies in the Deblois Granite (Sullivan et al., 2013). With increasing proximity to the center of the fault zone, these are: 1) a foliated granite domain, 2) a domain of foliated granite cut by localized shear zones, and 3) a main ultramylonite domain (Sullivan et al., 2013). The general abundance of minerals and bulk geochemistry of these rocks

remains relatively constant throughout these domains, indicating little to no fluid flux during deformation (Sullivan et al., 2013).

The foliated granite domain is the farthest from the contact with the FRF in the center of the shear zone (Fig. 2). This domain has an across-strike width of about 3 km, and is characterized by a general increase in foliation intensity approaching the main shear zone. The solid-state foliation is defined by elongated biotite and quartz grains and, in some places, aligned and flattened feldspar grains. The foliation is subvertical to steeply southeast dipping, and it strikes north-south at the southern margin of this domain. The strike progressively becomes 030-040° near to the main ultramylonite domain (Wang, 2007; Sullivan et al., 2013). The foliated granite exhibits microstructural evidence for dynamic recrystallization of quartz under amphibolite-facies temperatures, and an absence of solution transfer in quartz. The quartz is entirely recrystallized and forms irregularly shaped grains that exhibit 50-500-μm -wide subgrains. Feldspars appear to have deformed by simultaneous solution-precipitation and dislocation creep. These observations indicate that the bulk rheology in this domain was governed by the dislocation creep of quartz (Sullivan et al., 2013).

The localized shear zone domain is characterized by foliated granite cut by discrete, anastomosing mylonite and ultramylonite zones ranging in width from 2 mm to 1.5 m (Sullivan et al., 2013). Almost all of the localized shear zones exhibit both gradational and abrupt boundaries. The latter shows evidence for discrete fracture surfaces truncating individual mineral grains in the foliated granite. The shear zones strike north-northeast to east-northeast and dip moderately to steeply to both the northwest and the southeast. They contain both mylonite and ultramylonite, and they always cut the foliation in the granite indicating a later strain localization phase (Sullivan et al., 2013).

In localized shear zones cutting the foliated granite, mylonite is poorly mixed and exhibits clear domains of recrystallized quartz, feldspar and biotite (Sullivan et al., 2013). Quartz stringers and pods are 20-100% recrystallized, and they display sweeping undulose extinction (Sullivan et al., 2013). Relict quartz grains are comprised of subgrains, which concentrate at the boundaries. These data indicate that quartz in the localized shear zones experienced subgrain-rotation dynamic recrystallization (Sullivan et al., 2013). Ultramylonite in the localized shear zones has a matrix with relatively little quartz and more biotite, as compared with the granite protolith. Quartz ribbons and pods (10-100 μm in width) are prevalent in the ultramylonite matrix, and feldspar porphyroclasts (30-150 μm in width) are sparsely distributed throughout the matrix (Sullivan et al., 2013). Quartz in the ultramylonite matrix is 100% recrystallized, and feldspars exhibit grain-boundary bulges into adjacent grains of variable composition (Sullivan et al., 2013). At high magnification, 10-80-μm-wide compositional bands containing 10-80% biotite are evident. Biotite exhibits shape-preferred orientation parallel to compositional layering, although individual grains can have irregular branching shapes (Sullivan et al., 2013).

The abundance of small shear zones generally increases approaching the main ultramylonite zone. Deformed and recrystallized pseudotachylyte or ultracataclasite is evident in some of the localized ultramylonite zones. These observations all indicate that brittle-fault rocks localized ductile deformation, and they indicate that a short-lived phase of brittle deformation was responsible for creating them (Sullivan et al., 2013).

The main ultramylonite domain lies in the center of the KFZ. This contains two distinct facies, homogeneous and pinstripe ultramylonites. The contact between the main ultramylonite and localized shear zone domains occurs over a progressive gradient of 2 to 5 m as the small shear zones coalesce (Sullivan et al., 2013). The homogeneous ultramylonites resemble those

from the localized shear zone domain, but have quartz grains dispersed throughout the matrix, typically as 10-50-μm-wide, quartz-rich bands, but also as isolated grains (Fig. 3A). The quartz stringers are more elongate than those in localized shear zone domain ultramylonites, but they also show evidence for subgrain-rotation recrystallization (Sullivan et al., 2013). Feldspar porphyroclasts are rounded and have tails of recrystallized material that grade into the matrix (Fig. 3B). These matrix textures in the homogenous ultramylonite indicate deformation by granular flow, and are similar to those seen in the pinstripe ultramylonite (Sullivan et al., 2013).

Although the deformation mechanisms are similar, the pinstripe ultramylonites show compositional layering between quartz ribbons that are 50-100% recrystallized and feldspar ribbons, and they lack the ultra-fine-grained mixed matrix seen in homogenous ultramylonites (Fig. 3C). Sullivan et al. (2013) interpret these pinstripe ultramylonite as the remnants of foliated granite that underwent prolonged solid-state ductile deformation. Recrystallized quartz grains exhibit sweeping undulose extinction, deformation lamellae, and subgrains. These all indicate subgrain-rotation recrystallization (Fig. 3D) (Sullivan et al., 2013). Feldspar domains in the pinstripe ultramylonite are fractured, irregularly shaped, and display patchy and undulose extinction (Fig. 3E). Boundaries of relict feldspar grains are variable, and some boundaries are sharp and may be outlined with biotite seams or pressure-shadow overgrowths. Other relict feldspar grains have sutured boundaries rimmed by 1-5-μm-wide neoblasts indicating bulging recrystallization (Sullivan et al., 2013). All microstructural evidence from both ultramylonite types indicates that the long-term rheology of the main ultramylonite domain was governed by granular flow in the homogenous ultramylonites (Sullivan et al., 2013).

3. Methods

The current research project consisted of both field-and-laboratory components. Fieldwork took place during the 2011, 2012, and 2013 field seasons, and was primarily based on the preexisting bedrock geologic map of Fletcher Peak 7.5' Quadrangle by Wang (2007) as modified by Sullivan et al. (2013). The majority of the outcrops of FRF cut by the KFZ are along the shore of Third Machias Lake (Ludman, 1997; Wang, 2007). Out of 27 field stations, I collected ten oriented samples from eight field stations for thin section analysis (Fig. 2, Appendix). These samples are representative of an across-strike transect approaching the main shear zone. The transition zone between the foliated FRF and the mylonitic FRF is very poorly exposed due to glacial till cover. In addition, we discovered a 0.5-m-wide mylonitic granite dike at station three (Fig. 2, Appendix). I collected three samples across this dike and compared the deformation mechanisms in the dike to those of the Deblois Granite.

Laboratory analyses were conducted on FRF samples collected during the 2013 field season and granite samples collected in 2012 and 2011. Samples were chosen to provide the best representation across the shear zone given the limitations of exposure, and were cut perpendicular to foliation and parallel to the gently plunging lineation. These measurements were marked on hard samples in the field. Non-lineated samples were cut parallel with the strike of foliation. Polished thin sections were made by Spectrum Petrographics Inc in Vancouver, Washington. Thin sections were examined using a Hitachi S-2700 scanning electron microscope (SEM) and transmitted light microscope at Colby College in Waterville, Maine to look for evidence of: 1) dislocation creep regimes that operated in quartz aggregates (Stipp et al., 2002), 2) solution transfer and fluid movement during deformation (Hippertt and Hongn, 1998; Passchier and Trouw, 2005), 3) sliding on a grain boundary scale (Passchier and Trouw, 2005),

and 4) brittle deformation and overprinting by subsequent ductile deformation (Goodwiin and Wenk, 1995; Price et al., 2012; Sullivan et al., 2013). An energy dispersive X-ray spectrometer (EDS) on the SEM was used for grain-by grain spot checks of mineral composition in gold-coated, polished thin sections, in small areas to determine the mineralogy of specific domains and help identify phases in ultra fine-grained material.

4. Field Relationships

4.1 Foliated Flume Ridge Formation Outside the KFZ

The foliated Flume Ridge Formation lies outside of the KFZ to the northwest, and contains alternating beds of siltstone fining upwards to the northwest to mudstone, interpreted to represent turbidite sequences (Ludman, 1997; Ludman and Gibbons, 1999; Wang and Ludman, 2004; Wang, 2007). The beds strike 040-060° and are subvertical to steeply northwest dipping. The turbidite sequences range from 8-20 cm in thickness, and fine-grained beds contain foliation that formed during regional chlorite-grade metamorphism and tight folding (Ludman 1997; Wang and Ludman 2004, Wang, 2007). The coarse-grained beds show visible cleavage refraction with cleavage in these beds at a 20^{o} angle to original bedding and foliation in the fine-grained beds. Late-stage calcite veins are dispersed throughout the FRF. These veins are 1–10 mm thick and 20-70 cm in length, and they typically lie at about 60^{o} to foliation. Fine-grained beds also contain occasional visible quartz ribbons approximately 1 mm thick and 10 cm long. Other mineral phases are difficult to distinguish in the field.

4.2 Transition between deformed Flume Ridge Formation and Mylonitic Flume Ridge Formation

The complete transition from weakly deformed FRF to mylonitic FRF is not exposed due to glacial till cover. Two road outcrops, field stations 19 and 20, in the northeast corner of the field area, of FRF are less deformed than the mylonitic FRF but more deformed than the foliated FRF that lies outside the main shear zone (Fig. 2, Appendix). A progressive transition from the foliated FRF to the mylonitic FRF was visible in the samples collected at field stations 19 and 20. This inferred transition zone still contains visible turbidite sequences fining upwards to the northwest. Foliation in all rock layers strikes about 055, and is subvertical to steeply northwest dipping. Quartz veins range in width from 0.3-7.0 mm, are prevalent, and are concentrated in pelitic layers. They often display buckle folds and/or boudins, and pelitic layers are visibly more intensely foliated than the coarser-grained layers (Fig. 4).

4.3 Mylonitic Flume Ridge Formation

The mylonitic Flume Ridge Formation appears in a 500-m-wide belt in the center of the KFZ (Fig. 2). It is more homogenized than the foliated FRF at field stations 19 and 20 in the inferred transition zone, but relict bedding is faintly visible on fresh surfaces. There is no abrupt contact between the foliated FRF and the mylonitic FRF but, instead, this transition appears to occur over a progressive gradient. Micas become more abundant approaching the mylonite zone, and the Flume Ridge Formation becomes increasingly phyllitic in a southeast direction towards the center of the shear zone. Individual mineral grains are hard to distinguish in the mylonitic matrix in hand samples near the center of the shear zone, but macroscopic quartz veins become increasingly common in mylonitic FRF approaching the center of the KFZ. These veins are concentrated in pelitic layers and are typically boudinaged, with individual boudins completely pulled apart. Foliation is nearly vertical, but dips slightly to the northwest and strikes 040-060,

parallel to bedding and foliation of the foliated FRF outside the shear zone and the foliation of the mylonitic Deblois Granite on the southeast side of the zone. Mineral lineations are faintly visible on some foliation surfaces at field station 10, and are defined by streaking of mica-rich domains; micas plunge at approximately 43^{o}. All other FRF rocks cut by the KFZ are S-tectonites. Late stage kink-banding is abundant, and increases in prevalence approaching the center of the shear zone.

4.4 Mylonitic Granite Dike

The mylonitic dike at field station 3 lies parallel to foliation in the FRF. It strikes at 054°, is subvertical, and is 30 cm wide across strike (Fig. 2, Appendix). Faintly visible compositional banding progresses across strike in the dike, and local, completely pulled-apart, ~4-cm-long quartz boudins are parallel with foliation. Distinct subhorizontal lineations are visible on foliation surfaces. The dike has abrupt contacts with the FRF and appears relatively straight-edged, but may portray slight pinch-and-swell structure over its entire exposed length (Fig. 5). Other than quartz ribbons, individual mineral grains are indistinguishable in hand sample. There are some smaller mylonitic granite intrusions elsewhere in this outcrop, but these are all deformed and truncated by late-stage faults oblique to the foliation.

5. Microstructure

5.1 Flume Ridge Formation Outside the KFZ

In the Flume Ridge Formation to the northwest of the KFZ, optical microscopy combined with SEM revealed the following phases in order of decreasing abundance: quartz, Ca-rich plagioclase, potassium feldspar, biotite, epidote, and white mica. Plagioclase appears as isolated relict grains intergrown with sericite, potassium feldspar, white micas, epidote, and chlorite

(Figs. 6A, 6B). SEM analyses indicate that around these relict grains, minerals in pressure-shadow overgrowths have a lower concentration of calcium but prevalent peaks of potassium, aluminum, and some sodium. Minerals consist of potassium feldspar, muscovite, biotite, and epidote. Quartz is dispersed throughout the matrix in isolated 10-300-μm-wide, rounded grains, that are slightly elongate parallel to the foliation (Figs. 6A, 6B). The relict quartz grains exhibit sweeping undulose extinction and subgrains that are 10-50-μm wide, as well as dissolution seams on foliation-parallel faces and pressure-shadow overgrowths containing sheet silicates (Figs. 6A, 6B). Anhedral potassium feldspar is abundant in the pressure shadow overgrowths on the Ca-rich plagioclase, and shows no evidence of lattice distortion or dynamic recrystallization. Micas are typically present together in foliation-parallel dissolution seams bordering quartz and relict plagioclase grains.

5.2 Transition between deformed Flume Ridge Formation and Mylonitic Flume Ridge Formation

Rocks from the transition zone between weakly deformed FRF and mylonitic FRF exhibit two distinct compositional layers: 1) beds with an ultra-fine-grained matrix of recrystallized minerals, and 2) beds with fine-grained recrystallized matrix surrounding small quartz clasts. Micas are the dominant minerals in the ultra-fine-grained matrix, but quartz is present in 100-300-μm-wide pods, or extensively pulled apart, boudinaged quartz veins (Figs. 7A, 7B). Boudinaged veins are 50-100% recrystallized and exhibit sweeping undulose extinction from samples recovered closer to the center of the grain and subgrains. Coarser-grained areas contain quartz clasts that are rounded, elongate, and oriented parallel to foliation. Relict quartz clasts are 60-100% recrystallized and range from 20-50 μm in diameter. Most of the clasts show a polygonized texture of subgrains, and all portray sweeping undulose extinction. Grain

boundaries are distinct, and exhibit foliation-parallel dissolution seams that are primarily composed of micas (Figs. 7A-7C). Micas also grew in pressure-shadow-overgrowth tails and in dilatational sites between mechanically disaggregated grains in recrystallized tails. These grade progressively into the surrounding matrix (Figs. 7A-7C). This mixing texture occurs in both the finer-grained andcoarser grained beds, but is more pronounced in the coarser-grained beds. Evidence for brittle deformation is prevalent in this zone.

Pseudotachylyte injection and fault veins and bands of cataclasite that lie parallel to foliation directly adjacent to pseudotachylyte veins indicate a phase of brittle deformation (Figs. 7D, 7E). Pseudotachylyte contains circular quartz clasts that are up to 5 μm in diameter, and are preferentially preserved. These clasts have abrupt contacts with the surrounding pseudotachylyte matrix (Figs. 7D, 7E). Cataclasite in this zone contains rounded clasts of foliated, fine-grained matrix (Figs. 7D, 7E).

Potassium feldspar in the transition between deformed FRF and mylonitic FRF is entirely concentrated in multiple stages of syndeformational veins, many of which were rotated into the field of shortening. Veins at a high angle to foliation show discrete offset on foliation surfaces and bedding planes. These discrete shear offests commonly exhibit dilatational jogs with potassium feldspar and/or calcite infill (Fig. 7F). I found no potassium feldspar in the matrix in this domain.

5.3 Mylonitic Flume Ridge Formation

The FRF exhibits a progressive strain gradient from the transition zone to the center of the KFZ from the northwest to southeast. Based on SEM analyses, mineral phases in the mylonitic FRF are plagioclase, quartz, biotite, phengite, epidote, and chlorite. A fine-grained,

mica-rich, recrystallized matrix dominates the mylonitic FRF, but it also contains alternating 0.1-0.8-mm-wide bands with and without relict quartz clasts. These relict grains range in size from 10-100 μm, and most are 60-100% recrystallized. Quartz clasts exhibit prevalent sweeping undulose extinction and have a polygonized subgrain texture (Fig. 8A). These clasts make good shear sense indicators: they are pinched out, elongate, and commonly have sigma-shaped, foliation-parallel, mica-capped tails that step up in the direction of shear. There are a few relict Ca-rich plagioclase grains mixed with the relict quartz clasts, and they exhibit extensive replacement by phengite. Ca-rich plagioclase is more commonly present as 10–70-μm-wide subhedral grains mixed with quartz or intertwined with micas, and is elongate parallel to foliation.

Individual mineral phases in the fine-grained matrix are mostly indistinguishable under the light microscope. This matrix is predominantly elongate, subhedral phengite, chlorite, and biotite that ranges in size from 5-30 μm. Larger grains of phengite are one of the predominant minerals defining foliation, but smaller, 5-10-μm-long grains are oriented randomly and branch off of larger grains at sharp angles of 45-90^{o}, giving a bent appearance to larger grains (Fig. 8C). These smaller branches occur preferentially along grain boundaries with network silicate phases and have high axial ratios compared to other mineral phases. The sheet-silicate cleavage planes are oriented in the same direction and help define the dominant foliation (Fig. 8B, 8C). Quartz and plagioclase in the finer grained matrix exhibit foliation-parallel dissolution seams composed of phengite and biotite. These sheet silicates also grew similarly to those in the transition zone, as pressure-shadow overgrowths and in dilatational sites. The pressure-shadow overgrowths grade progressively into the finer grained matrix creating an interfingering texture.

Relict quartz grains are slightly rounded, elongate, and range in width from 10-20 μm. SEM analyses indicate quartz is less abundant in the fine-grained regions than in the coarse-grained regions. Quartz is also concentrated in 20-70-μm-wide ribbons parallel to foliation, and the ribbons are 80-100% recrystallized. Ribbons are boudinaged, and boudin structures range from pinch-and-swell structures to completely pulled-apart trains. Potassium feldspar is absent in the matrix, but is present in multiple stages of veins oriented anywhere at an angle from about 90^{o} to foliation to parallel with foliation (Figs. 8D, 8E). These veins display a slight pinch-and swell-structure when at high angles to foliation, but can be folded or completely pulled apart when oriented parallel with foliation. Feldspar-vein boundaries have jagged edges with seams of epidote around the veins, although the internal structure shows little deformation. The veins often are located in dilatational jogs in discrete slip surfaces (Fig. 8E). These slips occurred on discrete bedding planes or foliation surfaces, and cuts most other structures in these rocks. Foliation fish are present in the fine-grained matrix in this region, and act as clasts (Fig. 8F).

5.4 Mylonitic Granite dike

The mineralogical phases in the mylonitic dike are segregated into compositionally different bands. The SEM reveals that primary mineral phases are albite, muscovite/phengite, and quartz. Phengite-rich layers of interconnected phylosilicates lack potassium feldspar. Layers dominated by quartz and plagioclase lack abundant phengite and contain some potassium feldspar, which is often concentrated in veins. Quartz in the mylonitic dike is concentrated in 40-250-μm-wide ribbons parallel with foliation. These quartz ribbons are 90–100% recrystallized (Figs. 9A-9C). The ribbons also have a pinch-and-swell structure and progressively grade into plagioclase and potassium feldspar bands at their margins. Plagioclase in the dike is primarily

oligoclase, but a few rounded, relict albite grains are dispersed throughout the matrix along the boundaries of the quartz ribbons. These can be up to 100 μm in width (Fig. 9D). These relict albite grains exhibit replacement with oligoclase, are outlined by seams of phengite that have a fibrous appearance, and are aligned in interconnected layers (Fig. 9D). Potassium feldspar veins are dispersed in layers lacking phengite, and progressively grade into the quartz-and oligoclase-rich matrix.

6. Discussion

6.1 Significance of the Foliated Flume Ridge Formation Outside the KFZ

The foliated FRF outside of the main shear zone is the protolith to the mylonitic FRF based on field relationships. It was initially deformed under greenschist-facies conditions during the Late Silurian to Early Devonian phase of the Acadian orogeny in this region (Ludman, 1997; Wang and Ludman, 2004). This resulted in a composition of primarily Ca-rich plagioclase, quartz, biotite, and epidote (Wang and Ludman, 2004; Wang, 2007). The history of deformation is documented in both the quartz microstructure and the chemical reactions that occurred between the plagioclase, micas, and potassium feldspar that define the foliation. Prior to formation of the KFZ, dissolution seams around detrital quartz grains had surfaces normal to the principle shortening direction. Dissolved material reprecipitated locally as biotite and muscovite, forming beards and pressure shadows around the host grains (Figs. 6A, 6B). These textures indicate that an aqueous solution was present during deformation to accommodate local mass transfer (Wintsch and Yi, 2001). Quartz also shows mechanical mixing with potassium feldspar, which is one of the driving factors identified as indicative of strain softening in metasedimentary rocks (Wintsch et al., 1995, 2001, 2013; Wallis et al., 2013).

Original detrital plagioclase grains are Ca-rich, and show evidence of chemical alteration and replacement by sericite (Figs. 6A, 6B). Potassium feldspar, which is the primary mineral in the pressure-shadow overgrowths on Ca-rich plagioclase, shows no evidence of recrystallization. Alteration reactions occurred as aqueous fluids moved through the rocks and acted to modify chemical, mineralogical, and isotopic compositions (Wintsch et al., 1995). During Silurian regional metamorphism, reactions with a potassium-rich fluid must have caused the detrital Ca-rich plagioclase and the biotite to become metastable. A reaction occurred producing potassium feldspar, epidote, and muscovite. This reaction is noted by Wintsch et. al (2005):

biotite + plagioclase + quartz + K^+ + H_2O → epidote + potassium feldspar + muscovite + more-phlogopite-rich biotite

Calcium from plagioclase may have been concentrated in calcite veins, but XRF analyses indicate that white mica has an insignificant paragonite component. So, sodium is no longer prevalent, and this indicates that these reactions occurred in an open system. Additionally, the reaction precipitates micas that are elongate and parallel to the direction of foliation.

When oriented, mica strength is an order of magnitude less than that of both quartz and feldspar, and rock strength decreases as mica content increases (Wintsch et al., 1995). Additionally, experiments have demonstrated that muscovite is frictionally weaker than biotite (Wallis et al., 2013); therefore, an increase in abundance of phengite can effectively lower the long-term shear strength of the bulk rock (Wallis et al., 2013). The nucleation and growth of these new phengite grains in the FRF also reduced grain size and the strength of the rock because diffusion pathways around grains are shortened, and oriented mica grains enhance diffusion

parallel with foliation (Farver and Yund, 1999; Kilian et al., 2011). Therefore, the precipitation of micas and potassium feldspar prior to the formation of the KFZ is interpreted to have weakened the protolith of the mylonitic rocks, and created a series of weak zones, the pelitic layers, parallel to the incipient fault zone.

6.2 Significance of the transition between deformed Flume Ridge Formation and Mylonitic Flume Ridge Formation

The transition zone between the deformed FRF and the mylonitic FRF is dominated by a fine-grained matrix that lacks potassium feldspar and has abundant biotite and phengite. This matrix mineralogy probably formed via a reaction softening mechanism from a fluid-dominated system resulting in micas, feldspars and quartz dissolution and reprecipitation in dilatational sites with surfaces normal to the principal shortening direction (Wintsch et al., 1995; Wintsch and Yi, 2001). In the presence of excess fluid at temperatures of 350 ^{o}C and pressures ranging from 16-22 kbar, potassium feldspar will react with the phlogopite component of biotite to form phengite and a potassium- and magnesium-rich siliceous fluid (Massonne and Schreyer, 1987). This hydration reaction is noted by Wintsch et al. (1995 and 2005) and Massonne and Schreyer (1987):

Muscovite + potassium feldspar + quartz + phlogopite + H_2O = phengite + aqueous fluid rich in Fe and Mg

By increasing the phylosilicate content in the rock and decreasing the potassium feldspar content and volume, the rock becomes weaker than the protolith (Herwegh and Jenni, 2000; Wallis et al.,

2013). When shortened 45^{o} to the basal plane (001), phyllosilicates are significantly weaker and can deform by dislocation glide at low temperatures and shear stresses at any crustal level (Mares and Kronenberg, 1993; Wintsch et al., 1995). Experimental results also indicate that muscovite is weaker on (001) compared to biotite (Mares and Kronenberg, 1993). This indicates that the reaction-softening mechanism that produced the fine grained matrix and oriented phengite is a major weakening mechanism responsible for controlling the rheology of the FRF.

Additionally, oriented micas have Van der Waal bonding across layer interfaces. These interphase boundaries provide a channel for fluids, and energetically favor fluid films by drawing them along the basal layer interphases (Farver and Yund, 1999). Nano-scale fluid films are capable of supporting stress and reducing friction between the phengite layers, allowing grain boundary sliding to occur at low temperatures (Farver and Yund, 1999). These fluid channels are highly diffusive and, therefore, promote pressure solution in mineral aggregates and provide a pathway for material that dissolved under high stress to be transported and reprecipitated at interfaces under lower stress (Farver and Yund, 1999).

Quartz in this domain is found as small rounded clasts, in pods, or as entirely pulled-apart boudinaged veins (Figs. 7A-7C). The smaller clasts show sweeping undulose extinction, and the larger pods are 40-90% recrystallized by subgrain rotation and relict grains display clear sweeping undulose extinction (Fig. 7B). This indicates that the quartz in the transition zone deformed primarily by dislocation creep and recrystallized via subgrain rotation (Hirth and Tullis, 1992). Potassium feldspar veins that formed perpendicular to σ_3 at a high angle to foliation were deformed progressively and rotated into the field of shortening during progressive deformation.

Veins of pseudotachylyte and cataclasite correspond to late-stage brittle deformation that occurred during the final phase of the tectonic event. Late-stage potassium feldspar veins are pristine and experienced only localized slip on bedding planes and foliation surfaces indicating brittle failure, likely associated with late-stage deformation (Fig. 7F). Feldspar features are representative of late-stage strain hardening during the end of deformation. Potassium feldspar-filled dilatational jogs in discrete slip planes indicate that 1) fluid was present during this stage of deformation, and 2) this stage of deformation occurred in a shallower brittle regime (Sholz, 1988; Wallis et al., 2013). Veins occur as a result of overpressured pore fluids. The multiple stages of vein formation indicate that fluid pulsed in multiple stages throughout deformation during fault zone evolution in both the brittle and ductile regimes (Wallis et al., 2013). Pore pressure often reduces the effective normal stress, allowing for slip at lower shear stresses (Wallis et al., 2013). The absence of brittle deformation at low confining pressure and pore fluid pressure, until the later stages of the KFZ, indicates that differential stress is low (Wallis et al., 2013).

6.3 Significance of the Mylonitic Flume Ridge Formation

The mylonitic FRF is similar to the rocks in the transition zone, but appears to be more evolved. Relict quartz clasts and quartz boudins are distributed similarly, but they are fewer and smaller than in the transition zone. These smaller clasts show distinct evidence for dissolution-precipitation creep, such as foliation-parallel caps of mica and pressure-shadow overgrowths (Fig. 8A). Internally, these relict grains and boudinaged quartz veins are similar to those in the transition zone, but are 100% dynamically recrystallized by subgrain rotation and individual quartz grains exhibit patchy to sweeping undulose extinction. Sweeping undulose extinction and

subgrain-rotation recrystallization indicates dislocation climb to accommodate recovery (Hirth and Tullis, 1992). Therefore, quartz in these rocks is interpreted to have deformed by diffusional processes and dislocation creep (Hirth and Tullis, 1992; Stipp et al., 2002). However, quartz is not the weakest phase, and did not control the rheology of the FRF.

The combination of reaction softening, solution-transfer processes, and granular flow in the ultra-fine-grained polyphase matrix controls the rheology of the metasedimentary rocks in the mylonitic domain (Wintsch et al., 1995; Herwegh and Jenni, 2000; Wallis et al., 2013). With the addition of aqueous fluid, the combination of quartz, plagioclase, potassium feldspar, and biotite became metastable and reacted to form interconnected layers of phengite. Recrystallization of feldspar and nucleation of phengite preferentially initiated at grain boundaries (Figs. 8B, 8C). Nucleation is interpreted due to the presence of small grain size and idiomorphic grain shape of the mica, and can be induced by local variations in pore pressure or fluid chemistry (Fig. 8C) (Herwegh and Jenni, 2001). As in the other domains, interconnected layers of phengite promoted fluid flow and grain boundary sliding (Herwegh and Jenni, 2000). Myrmekite replacement is not evident, indicating that Ca-bearing plagioclase was not stable and unable to replace the potassium feldspar (Fitzgerald and Stunitz, 1993).

Evidence for late-stage strain hardening near the end of deformation, similar to that identified in the transition zone, is prevalent in the mylonitic FRF. Foliation fish are dispersed in the fine-grained matrix, and acted as clasts (Fig. 8F). Late-stage potassium feldspar veins record localized slip on bedding planes and foliation surfaces like those in the transition zone. These veins precipitated in dilatational jogs due to overpressure of pore fluids at shallow depths during the late stage brittle deformation phase (Figs. 8D, 8E).

6.4 Significance of the Mylonitic Granite dike

Deformation in the mylonitic dike is similar to deformation in the mylonitic FRF, and these rocks also exhibit extensive evidence for fluid flux during deformation. Segregated quartz and plagioclase regions that host potassium feldspar veins exhibit extensive mechanical mixing, effectively reducing the strength of the rock. This is similar to the mechanism described by Kilian et al. (2011) (Fig. 9D). Quartz is concentrated into ribbons, likely from the elongation of original igneous quartz grains as opposed to being concentrated by reaction-softening processes like those in the mylonitic FRF. This interpretation is based on optical microscopy data that indicates the quartz is 100% recrystallized by subgrain rotation and shows patchy undulose extinction. These textures indicate that the quartz deformed primarily by dislocation creep (Figs. 9B, 9C) (Hirth and Tullis, 1992). Few relict albite clasts are dispersed throughout the matrix and these exhibit dissolution seams normal to the principal shortening direction. Phengite and plagioclase have reprecipitated locally, forming beards around the feldspar grains, parallel to foliation. Beards of reprecipitated minerals are mechanically mixed with the surrounding matrix, weakening the overall strength of the rock (Fig. 9D) (Kilian et al., 2011). These indicate an aqueous solution was present to accommodate local mass transfer during deformation (Hirth and Tullis, 1992; Stipp et al., 2002; Kilian et al., 2011).

6.5 Deformation Mechanisms in the Deblois granite vs. Mechanisms in the FRF

Fluid flux did not play a role in the mechanisms that governed deformation in the Deblois granite (Sullivan et al., 2013). No chemical changes or veins and few dilatational sites in microstructure were observed, all of which would be expected in deformation influenced by fluid. Phase abundances and mineralogy are constant across the strain gradient, and reaction-

softening processes did not play a role in strain weakening. The rheology of the granite experienced a three-phase evolution: 1) the foliated granite primarily deformed by the dislocation creep of quartz, 2) the localized shear zones formed after phase mixing during a period of brittle deformation, and 3) the main ultramylonite primarily deformed by granular flow in the matrix catalyzed by phase mixing during the brittle phase (Sullivan et al., 2013). A brief phase of brittle deformation catalyzed the formation of both the localized shear zone domain and the main ultramylonite domain by grain size reduction and mechanical mixing, reducing the shear strength of the granite (Sullivan et al., 2013).

In contrast, the metasedimentary rocks of the FRF experienced abundant fluid influx throughout deformation, as indicated by significant alteration of minerals via syndeformational reactions, extensive precipitation of minerals in dilatational sites, formation of foliation-parallel pressure solution seams, and multiple generations of syndeformational veins. This fluid infiltration catalyzed a progressive deformation gradient across strike as opposed to distinct domains and abrupt strain gradients seen in the Deblois granite cut by the KFZ. Prior to formation of the KFZ, initial strain softening of the metasedimentary rocks occurred as a result of fluid flux related to contact metamorphism, which altered the chemical and mineralogical compositions, creating oriented micas that continued to enhance fluid movement. However, similar to the granite, the rheology of the mylonitic FRF was governed by granular flow and dissolution-precipitation creep in the ultra-fine-grained polyphase mixtures, which were primarily comprised of micas. Late-stage hardening of the mylonitic metasedimentary rocks is recorded by discrete slip on bedding planes and foliation surfaces and the presence of pseudotachylyte and cataclasite, as well as foliation fish. This most likely indicates a decrease in temperature.

7. Broader Implications

Many case studies indicate that chemical alteration plays a significant role in strain localization in the upper crust, (e.g., O'Hara, 1988; Fitzgerald and Stunitz, 1993). Exhumed fault rocks formed in the brittle-ductile transition can be used to further assess the strength of fault zones. Wallis et al. (2013) examined the metavolcano-sedimentary formations in the Karakoram Fault Zone in the northwest Himalaya. They found that reaction softening often resulted in the formation of well-developed, interconnected layers of chlorite, sericite, and phengite parallel to foliation that weakened the fault zone. These layers aided deformation by enhancing diffusive mass transfer. Additionally, multiple generations of veins indicated that fluid-flux pulsed throughout the evolution of the fault zone. Wallis et al.'s (2013) model for fault weakening mechanisms via reaction softening processes is similar to mine, although, despite the abundant evidence for fault-weakening mechanisms, this fault zone is currently locked and expected to produce a 7.5+ moment magnitude earthquake in the future.

Wintsch et al. (1995) found that in the presence of mineral-aqueous fluid, the phyllosilicate content of a rock will increase via feldspar weakening mechanisms, and will decrease the shear strength of fault zones if they form well-developed fabrics. They examined Mg-rich mafic rocks and found that replacement with biotite and chlorite can occur at both shallow and deep crustal regimes. Fault zones that contain high concentrations of phyllosilicates with preferred orientations can exhibit aseismic slip. Wintsch et al. (1995) also suggest that since the San Andreas Fault contains abundant Mg-rich rocks, these reaction softening processes may play a role in the weakness of the Fault. While my data do not examine Mg-rich mafic rocks, reaction softening processes were a major weakening mechanism in the FRF in the KFZ.

8. Conclusions

The mylonitic FRF exhibits a progressive strain gradient approaching the center of the KFZ. Fluid flux enhanced fault-weakening mechanisms that exploited weaker mineral phases in the FRF. Throughout the gradient of deformation, there is increased phase mixing in all layers, but mixing is most pronounced in the coarser layers. The rheology in the mylonitic FRF domain was controlled by granular flow and dissolution precipitation in the newly formed, ultra-fine-grained, polyphase mixtures, but these rocks initially underwent reaction softening as a result of fluid flux during an earlier contact metamorphic event. Quartz deformed by solution precipitation and dislocation creep, but was not the weakest phase. These deformation mechanisms in the FRF can potentially be used as an analogue for active strike-slip zones that may be experiencing weakening mechanisms at depth.

References

Bradley, D.C., Tucker, R.D., Lux, D.R., Harris, A.G., McGregor, C.D. 2000. Migration of the Acadian Orogen and foreland basin across the northern Appalachians of Maine and adjacent areas. United States Geological Survey, 1-49.

Chen, W.P., Molnar, P., 1983. Focal depths of intracontinental and intraplate earthquakes and their implications for the thermal and mechanical properties of the lithosphere. Journal of Geophysical Research 88, 4183–4214.

Farver, J.R., Yund, R.A. 1999. Oxygen bulk diffusion measurements and TEM characterization of a natural ultramylonite: implications for fluid transport in mica-bearing rocks. Metamorphic Geology 17, 669-683.

Fitzgerald, J.D., Stunitz, H. 1993. Deformation of granitoids at low metamorphic grade. I: Reactions and grain size reduction. Tectonophysics 221, 269-297.

Goldstein, A., Hepburn, J. C., 1999. Possible correlations of the Norumbega fault system with faults in southeastern New England In: Ludman, A. and West, D.P., Jr., (Eds.), The Norumbega Fault System of the Northern Appalachians. Geological Society of America Special Paper 331, 73–84.

Goodwin, L. B., Wenk, H. R., 1995. Development of phyllonite from granodiorite: Mechanisms of grain-size reduction in the Santa Rosa mylonite zone, California. Journal of Structural Geology 17, 689–707.

Handy, M. R., Hirth, G., Burgmann, R., 2007. Continental fault structure and rheology from the frictional-to-viscous transition downward. In: Handy, M. R., Hirth, G., Hovius, N. (Eds.), Tectonic faults: Agents of Change on a Dynamic Earth. MIT Press, Cambridge, Mass., USA, 139–181.

Herwegh, M., Jenni, A., 2001. Granular flow in polymineralic rock bearing sheet silicates: new evidence from natural samples. Tectonophysics 332, 309–320.

Hibbard, J., van Staal, C., Rankin, D., Williams, H., 2006. Lithotectonic Map of the Appalachian Orogen, Canada-United States of America. Geological Survey of Canada Map 02096A, scale 1:1500000.

Hippertt, J. F., Hongn, F. D., 1998. Deformation mechanisms in the mylonite/ultramylonite transition. Journal of Structural Geology 20, 1435–1448.

Holyoke, C. W., Tullis, J., 2006. Mechanisms of weak phase interconnection and the effects of phase strength contrast on fabric development. Journal of Structural Geology 28, 621–640.

Jackson, J., 2002. Strength of the continental lithosphere: time to abandon the jelly sandwich? GSA Today 12, 4–10, doi: 10.1130/1052-5173(2002)012.

Kilian, R., Heilbronner, R., Stünitz, H., 2011. Quartz grain size reduction in a granitoid rock and

the transition from dislocation to diffusion creep. Journal of Structural Geology 33, 1265–1284.

Kirby, W., 1985. Rock Mechanics observations pertinent to the rheology of the continental lithosphere and the localization of strain along shear zones. Tectonophysics 118, 1–27.

Ludman, A., Berry, H. N., IV, 2003. Bedrock Geology of the Calais 1:100,000 Quadrangle, Maine. Maine Geological Survey Open-File 03-97, scale 1:100,000.

Ludman, A., 1997. Evolution of a transcurrent fault system in shallow crustal metasedimentary rocks: the Norumbega fault zone, eastern Maine. Journal of structural geology 20, 93-107.

Ludman, A., Hopeck, J., Brock, P. C., 1993. Nature of the Acadian orogeny in eastern Maine. In: Roy, D. C., Skehan, J. W. (Eds.), The Acadian Orogeny: Recent Studies in New England, Maritime Canada, and the Autochthonous Foreland. Geological Society of America Special Paper 275, 67–84.

Ludman, A., West, D. P., Jr., 1999. Preface to: Norumbega Fault System of the Northern Appalachians In: Ludman, A. and West, D.P., Jr., (Eds.), The Norumbega Fault System of the Northern Appalachians. Geological Society of America Special Paper 331, v–xii.

Mares, V.M., Kronenberg, A.K., 1993. Experimental deformation of muscovite. Journal of Structural Geology 15, 1061-1075.

Massonne, H., Schreyer, W. 1987. Phengite geobarometry based on the limiting assemblage with K-feldspar, phlogopite and quartz. Contributions to Mineralogy and Petrology 96, 212-224.

Montési, L. G. J., 2013. Fabric development as the key for forming ductile shear zones and enabling place tectonics. Journal of Structural Geology 50, 254–266.

O'Hara, K., 1988. Fluid flow and volume loss during mylonitization: an origin for phyllonite in an overthrust setting, North Carolina, U.S.A. Tectonophysics 156, 21–36.

Osberg, P.H., Hussey II, A.M., Boone, G.M., 1985. Bedrock geologic map of Maine. Augusta, Maine Geologic Survey, scale 1:500,000.

Park, A. F., Whitehead, J., 2003. Structural transect through Silurian turbidites of the Fredericton Belt southwest of Fredericton, New Brunswick: the role of the Fredericton Fault in late Iapetus convergence. Atlantic Geology 39, p. 227-237.

Passchier, C.W., Trouw, R.A.J., 2005. Microtectonics. Springer-Verlag, Berlin.

Platt, J. P., Behr, W. M., 2011. Grain size evolution in ductile shear zones: implications for strain localization and the strength of the lithosphere. Journal of Structural Geology 33, 537–550.

Robinson, P., Tucker, R. D., Bradley, D., Berry, H. N., Osberg, P. H., 1998. Paleozoic orogens in New England, USA. Geologiska Föreningens i Stockholm Förhandlingar 120, 119–148.

Scholz, C.H. 1988. Earthquakes and friction laws. Nature 391, 37-42.

Sibson, R. H., 1977. Fault rocks and fault mechanisms. Journal of the Geological Society, London 133, 191–213.

Stipp, M., Tullis, J., 2003. The recrystallized grain size piezometer for quartz. Geophyiscal Research Letters 30, doi:10.1029/2003GL018444.

Stipp, M., Tullis, J., Scherwath, M., Behrmann, J. H., 2010. A new perspective on paleopiezometry: Dynamically recrystallized grain size distributions indicate mechanism changes. Geology 38, 759–762.

Sullivan W.A., Boyd A. S., Monz M.E., 2013. Strain localization in homogeneous granite near the brittle-ductile transition: A case study of the Kellyland fault zone, Maine, USA. Journal of Structural Geology, in press.

Thatcher, W., Pollitz, F. F., 2008. Temporal evolution of continental lithospheric strength in actively deforming regions. GSA Today 18, no. 4/5, doi: 10.1130/GSAT01804-5A.1.

Tullis, J., Yund, R. A., 1985. Dynamic recrystallization of feldspar: A mechanism for ductile shear zone formation. Geology 13, 238–241.

Wallis, D., Philips, R.J., Lloyd, G.E. 2013. Fault weakening across the frictional-viscous transition zone, Karakoram Fault Zone, NW Himalaya. Tectonics 32, 1227-1246.

Wang, C., 2007. Bedrock Geology of the Fletcher Peak 7.5' Quadrangle, Maine. Maine Geological Survey Open File 07-143, scale 1:24,000, 16

Wang, C., Ludman, A., 2004. Deformation conditions, kinematics, and displacement history of shallow crustal ductile shearing in the Norumbega fault system in the Northern Appalachians, eastern Maine. Tectonophysics 384, 129–148.

West, D. P., Beal, H. M., Grover, T. W. 2003. Silurian deformation and metamorphism of Ordovician arc rocks of the Casco Bay Group, south-central Maine. Canadian Journal of Earth Sciences 40, 887–905.

West, D.P., Roden-Tice, M.K. 2003. Late Cretaceous reactivation of the Norumbega fault zone, Maine: Evidence from apatite fission-track ages. Geology31, 649-652.

Wintsch, R.P., Aleinikoff, J.N., Yi, K. 2005. Foliation development and reaction softening by dissolution and precipitation in the transformation of granodiorite to orthogneiss, Glastonbury Complex, Connecticut, U.S.A. The Canadian Mineralogist43, 327-347.

Wintsch, R.P., Christoffersen, R., Kronenberg, A.K. 1999. Fluid-rock weakening of fault zones. Journal of Geophysical Research 100, 13021-13032.

Wintsch, R.P., Yeh, M., 2013. Oscillating brittle and viscous behavior through the earthquake cycle in the Red River Shear Zone: Monitoring flips between reaction and textural softening

and hardening. Tectonophysics 587, 46-62.

Wintsch, R.P., Yi, K. 2001. Dissolution and replacement creep: a significant deformation mechanism in mid-crustal rock. Journal of Structural Geology 24, 1179-1193.

Figure Captions

Figure 1: Simplified geologic map of Maine portraying major intrusive bodies, rock units, dextral strike-slip faults, and the study area of this project (Compiled from Osberg et al. 1985; Robinson et al., 1998; Goldstein and Hepburn, 1999; Ludman and Berry, 2003; West et al., 2003; Wang and Ludman, 2004; Hibbard et al., 2006).

Figure 2: Geologic map of the study area showing sample location of thin sections, the three different strain facies of the Deblois granite and where the KFZ cuts the FRF.

Figure 3: Gray-scale photomicrographs and SEM images from Sullivan et al. (2013) depicting textures and characteristic microstructures in the three different strain facies in the Deblois granite. (A) Cross-polarized-light image showing the typical microstructure of the homogeneous ultramylonite. (B) Back-scatter-electron image of homogenous ultramylonite depicting a tailed feldspar within the fine-grained matrix, and textural evidence for mechanical mixing of quartz and feldspar (red box). (C) Cross-polarized-light image of alternating quartz and feldspar ribbons in pinstripe ultramylonite. (D) Cross-polarized-light image depicting quartz recrystallization texture in pinstripe ultramylonites. (E) Cross-polarized-light image showing undulose and patchy extinction in relict feldspar grains.

Figure 4: Photographs highlighting the concentration of quartz veins in pelitic layers in the potential transition zone between weakly foliated and mylonitic FRF. Sample locations given in figure 2. Veins have structures such as (A) entirely pulled-apart shear band style boudins and (B) buckle folds that indicate they are stronger than the surrounding matrix. Penny used for scale.

Figure 5: Photograph depicting the mylonitic granitic dike located at field station 3 (Fig. 2). Drill holes show location of samples. FR03-E was not used for analyses due to extensive weathering and fracturing that caused the drill core to shatter.

Figure 6: Images showing microstructure in the foliated FRF outside the KFZ. Sample locations are given in figure 2. Mineral abreviations are: Qtz=quartz, Kfs=potassium feldspar, Bt=biotite, Phngt=phengite, Plg=plagioclase. (A) Backscatter-electron image of the foliated FRF matrix in sample collected at station 5. Image highlights the dissolution and precipitation of quartz and pristine potassium feldspar and mica. (B) Cross-polarized-light photomicrograph of a sample collected at station 6, that shows the typical microstructure in the foliated FRF. Replacement of plagioclase by sericite, and relatively pristine potassium feldspar are visible.

Figure 7: images showing the microstructure in the transition zone between foliated FRF and mylonitic FRF in the KFZ. Sample locations are given in figure 2. Mineral abreviations are: Qtz=quartz, Kfs=potassium feldspar, Bt=biotite, Phngt=phengite, Plg=plagioclase. (A) Backscatter-electron image of a sample collected at station 20. Image shows a pelitic layer that underwent dissolution-precipitation of quartz and extensive nucleation and growth of micas in randomly oriented directions between disaggregated quartz grains in the pressure-shadow tails on a quartz clast. (B) Cross-polarized photomicrograph of the same quartz clast depicted in A, showing dissolution seams on foliation-parallel faces, some evidence for subgrain rotation recrystallization and sweeping undulose extinction. (C) Backscatter-electron image of the fine-grained matrix in a sample collected at station 19. Image shows mixing of quartz and plagioclase. Note weak preferred orientation of most mica parallel with foliation, but some mica

depicts nucleation and growth in oriented directions between grains (red box). evidence for mixing between quartz and plagioclase (red box). (D) Cross-polarized-light image of cataclasite and pseudotachylyte injection veins in a sample collected at station 19. Cataclasite contains foliated relict matrix material. (E) Backscatter-electron image showing matrix in pseudotachylyte that contains rounded quartz clasts in a sample collected at station 19. (F) Cross-polarized-light image collected at station 19. Note discrete slip between potassium feldspar veins and matrix along bedding planes and foliation surfaces. These veins nucleated in dilatational jogs.

Figure 8: images depicting the microstructure of the mylonitic FRF. Sample locations are shown in figure 2. Mineral abreviations are: Qtz=quartz, Kfs=potassium feldspar, Bt=biotite, Phngt=phengite, Plg=plagioclase. (A) Backscatter-electron image collected at station 7 showing a quartz clast within the fine-grained matrix. The clast exhibits extensive pressure-shadow overgrowths. (B) Backscatter-electron image collected at station 2 showing mechanical mixing and chemical alteration between the phengite and the minute amounts of potassium feldspar in the fine-grained matrix. (C) Backscatter-electron image collected at station 10 depicting extensive nucleation and growth of micas in randomly oriented directions between grains within the matrix (red box i), and grains that nucleated and rotated into the plane of shear (red box ii). (D) Backscatter-electron image collected at station 7 showing a rotated potassium feldspar vein that exhibits mixing with quartz. (E) Cross-polarized-light image collected at station 10 showing discrete slip of a potassium feldspar vein on a bedding plane. (F) Cross-polarized-light image collected at station 10 showing a foliation fish (red box) and boudinaged quartz veins that are 100% recrystallized and are concentrated in the fine-grained matrix in pelitic bands.

Figure 9: Images depicting the microstructure in the mylonitic granitic dike collected at station 3 (fig. 2). Exact core location are marked on Figure 5. Mineral abreviations are: Qtz=quartz, Phngt=phengite, Plg=plagioclase, Ab=albite. (A) Cross-polarized-light image of core FR03-F depicting bands of fine-grained matrix that either contain abundant muscovite or potassium feldspar. Quartz ribbon is also present and shows subgrains. (B) Cross-polarized-light image of core FR03-G depicting a quartz pod that is entirely recrystallized by subgrain rotation and is in a muscovite-rich area. (C) Cross-polarized-light image depiof core FR03-H cting a quartz recrystallized ribbon. Note subgrains that are the same size as the recrystallized grains, indicating subgrain-rotation recrstallization. (D) Backscatter-electron image of core FR03-H showing a relict albite porphyroclast that has dissolution seams on foliation-parallel surfaces (red box), and exhibits mixing with more Ca-rich plagioclase in tails.

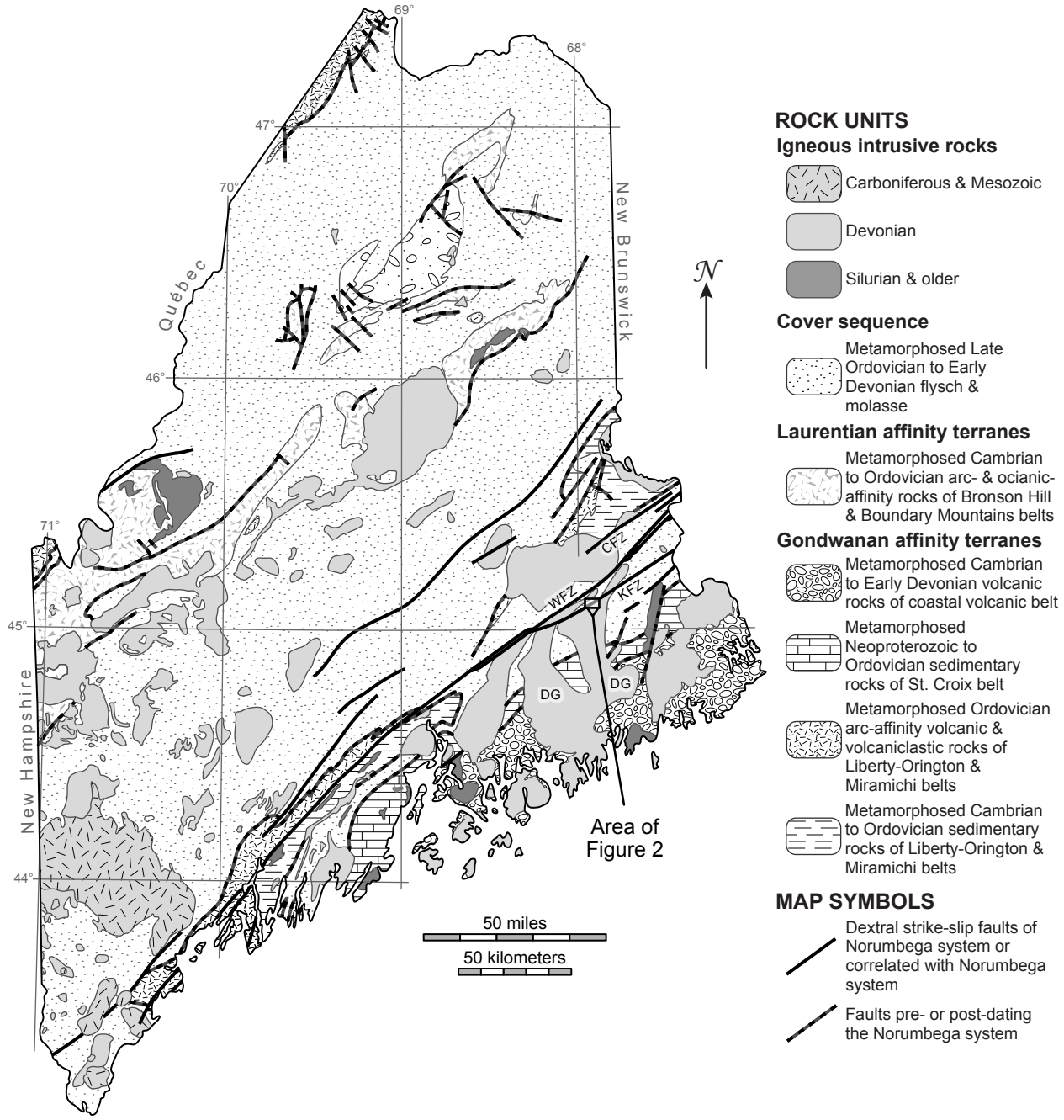
69°
68°
47°
70°
46°
71°
45°
44°
Québec
New Brunswick
New Hampshire
CFZ
WFZ
KFZ
DG
DG
Area of Figure 2
50 miles
50 kilometers
N
ROCK UNITS
Igneous intrusive rocks
Carboniferous & Mesozoic
Devonian
Silurian & older
Cover sequence
Metamorphosed Late Ordovician to Early Devonian flysch & molasse
Laurentian affinity terranes
Metamorphosed Cambrian to Ordovician arc- & ocianic-affinity rocks of Bronson Hill & Boundary Mountains belts
Gondwanan affinity terranes
Metamorphosed Cambrian to Early Devonian volcanic rocks of coastal volcanic belt
Metamorphosed Neoproterozoic to Ordovician sedimentary rocks of St. Croix belt
Metamorphosed Ordovician arc-affinity volcanic & volcaniclastic rocks of Liberty-Orington & Miramichi belts
Metamorphosed Cambrian to Ordovician sedimentary rocks of Liberty-Orington & Miramichi belts
MAP SYMBOLS
Dextral strike-slip faults of Norumbega system or correlated with Norumbega system
Faults pre- or post-dating the Norumbega system

Figure 1

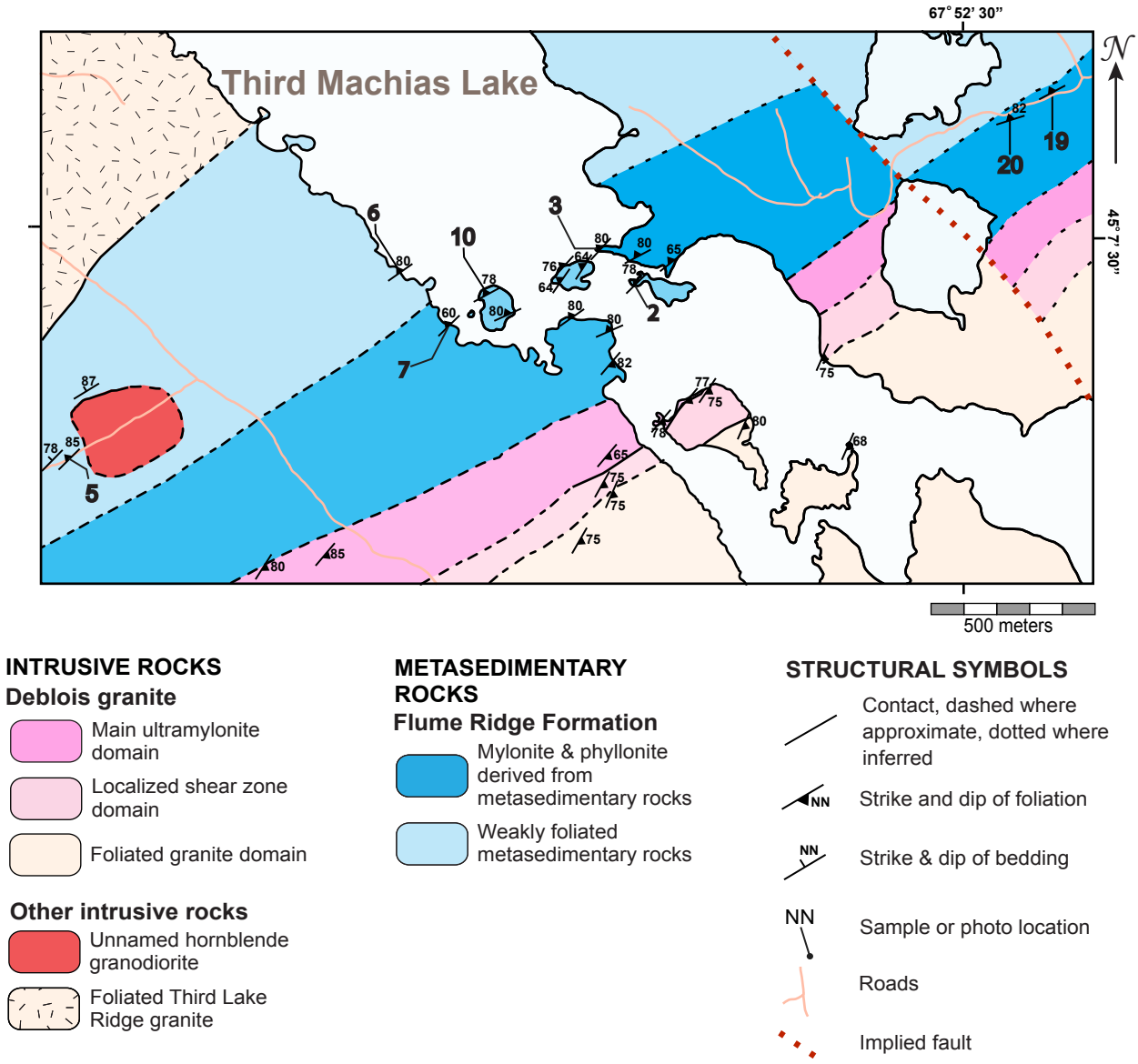
67° 52' 30"
45° 47' 30"
N
Third Machias Lake
500 meters
INTRUSIVE ROCKS
Deblois granite
Main ultramylonite domain
Localized shear zone domain
Foliated granite domain
Other intrusive rocks
Unnamed hornblende granodiorite
Foliated Third Lake Ridge granite
METASEDIMENTARY ROCKS
Flume Ridge Formation
Mylonite & phyllonite derived from metasedimentary rocks
Weakly foliated metasedimentary rocks
STRUCTURAL SYMBOLS
Contact, dashed where approximate, dotted where inferred
Strike and dip of foliation
Strike & dip of bedding
Sample or photo location
Roads
Implied fault

Figure 2

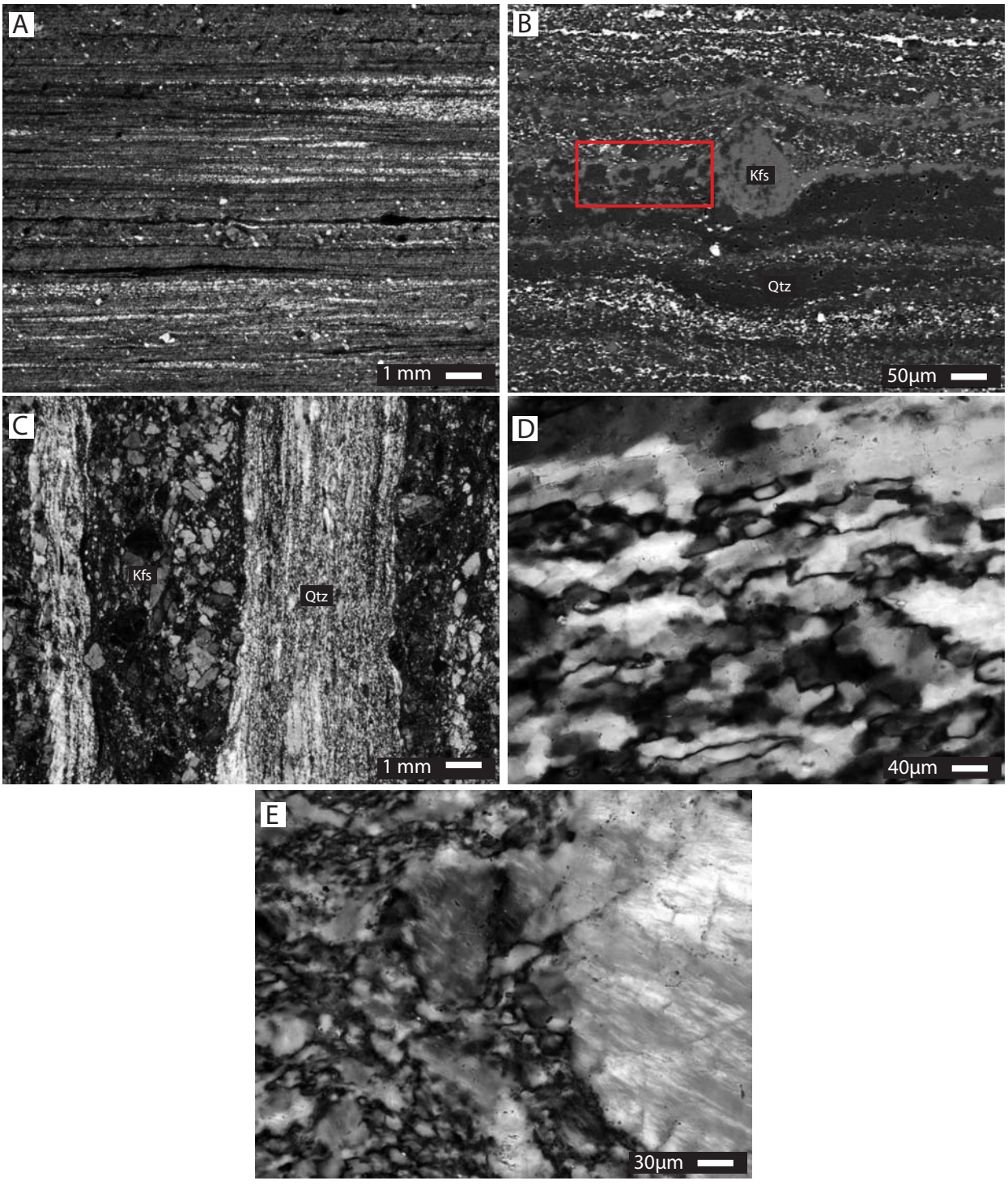

Figure 3

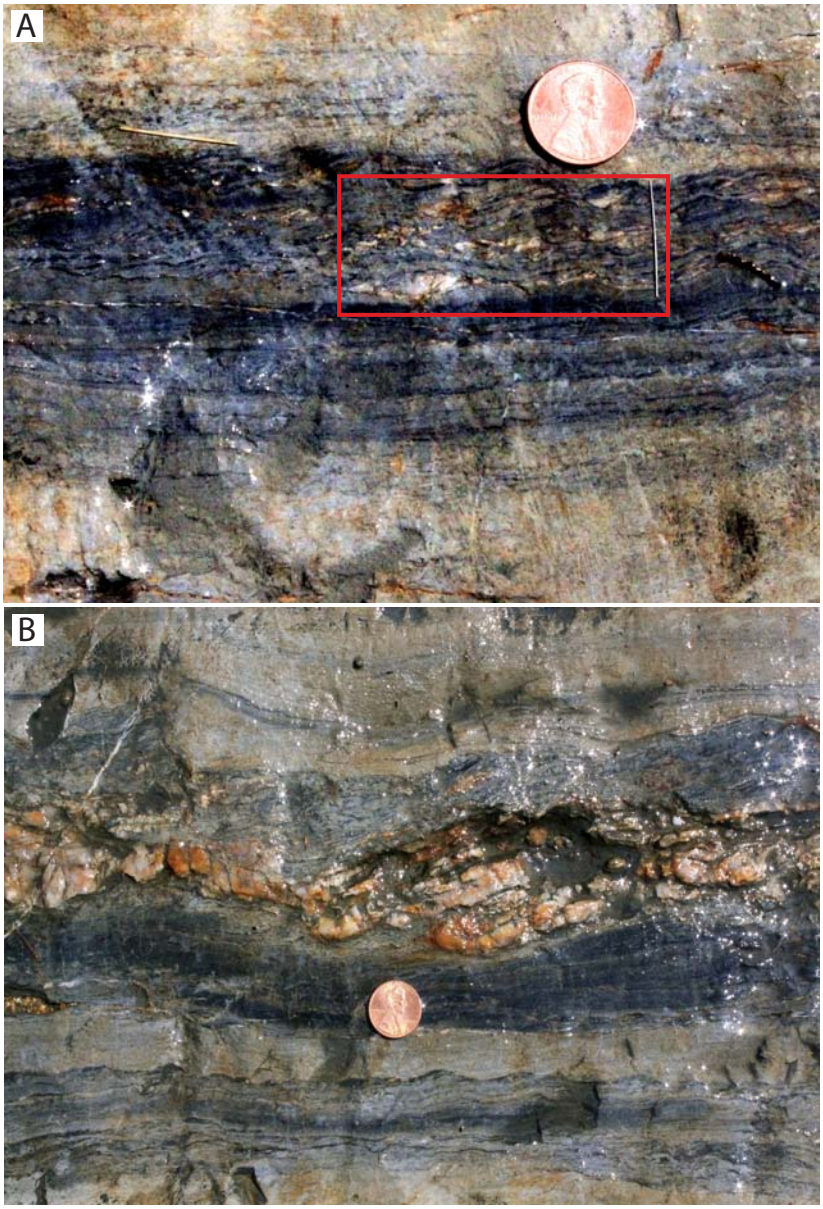

Figure 4

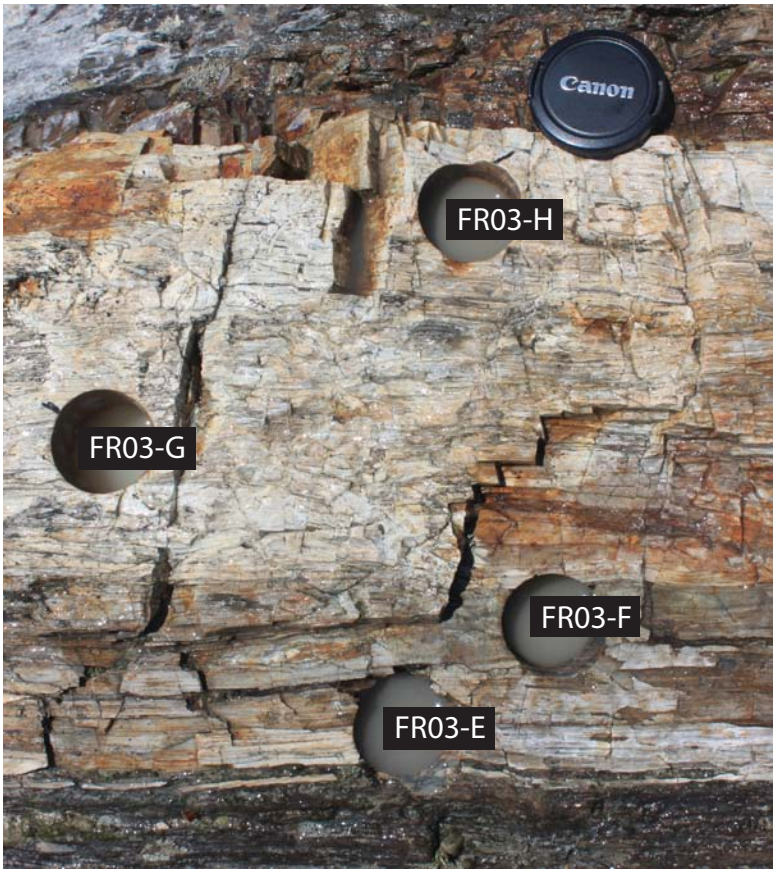

Figure 5

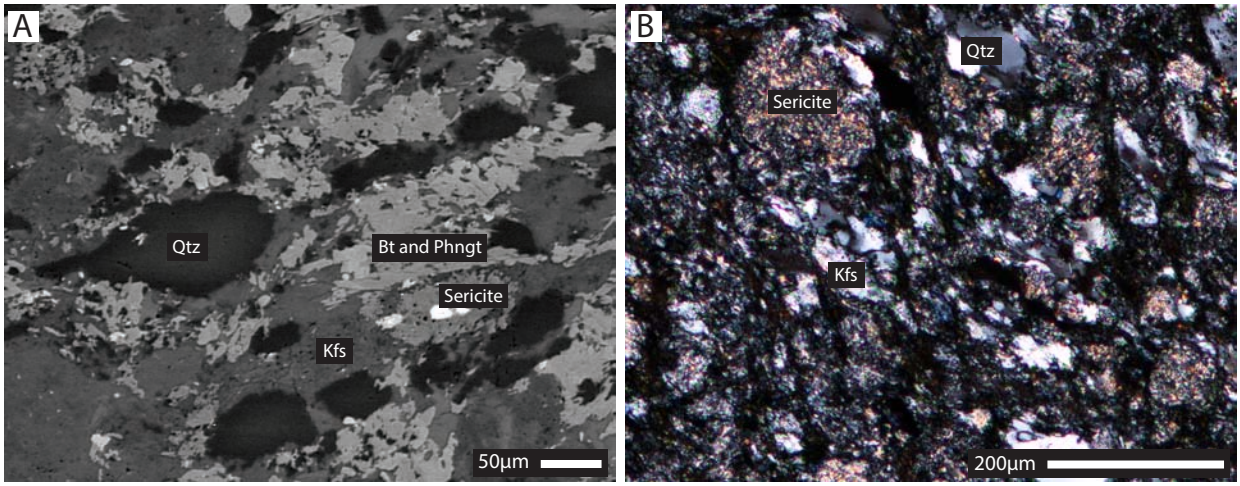

Figure 6

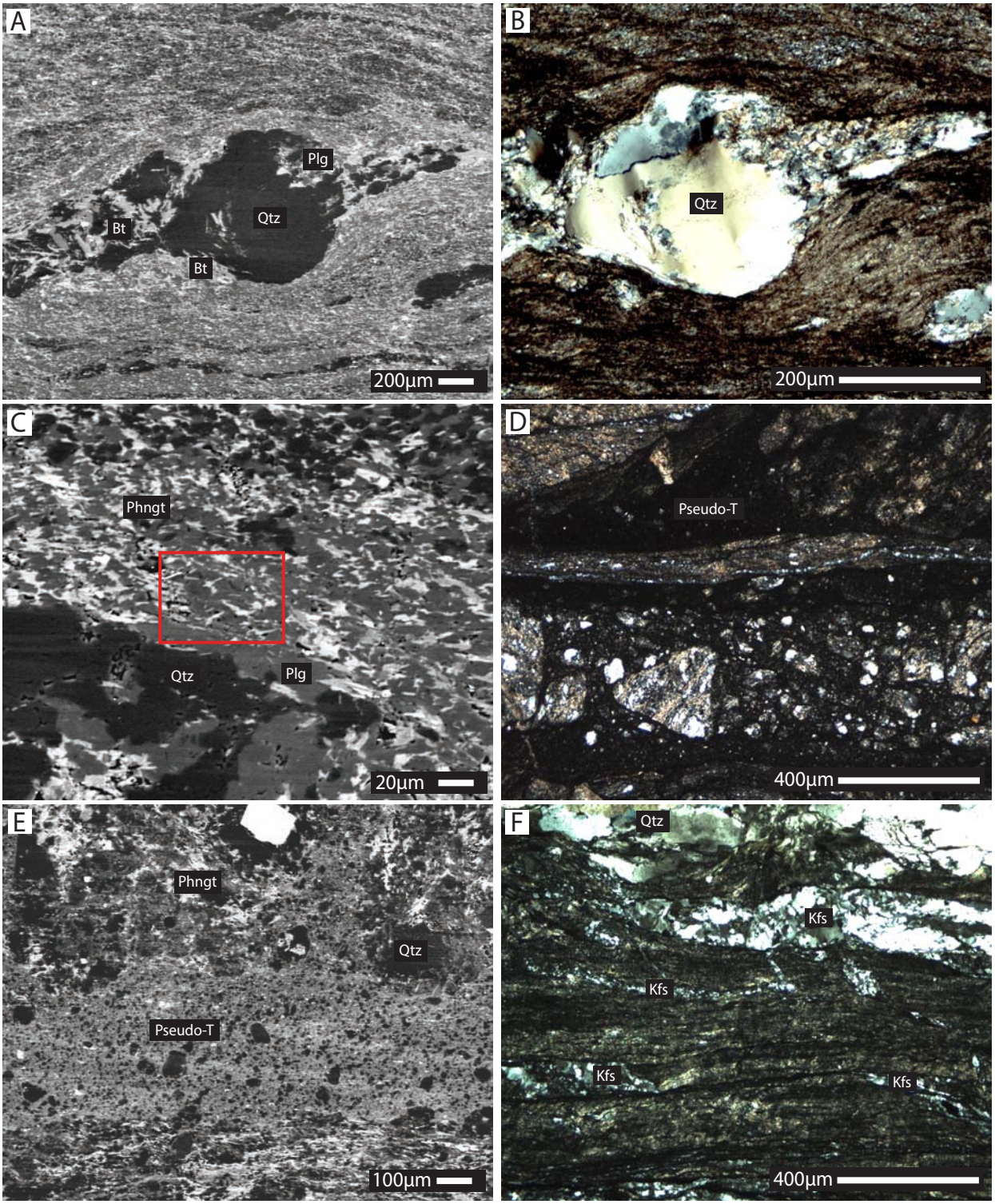
A
Plg
Qtz
Bt
Bt
200µm
B
Qtz
200µm
C
Phngt
Qtz
Plg
20µm
D
Pseudo-T
400µm
E
Phngt
Qtz
Pseudo-T
100µm
F
Qtz
Kfs
Kfs
Kfs
Kfs
400µm

Figure 7

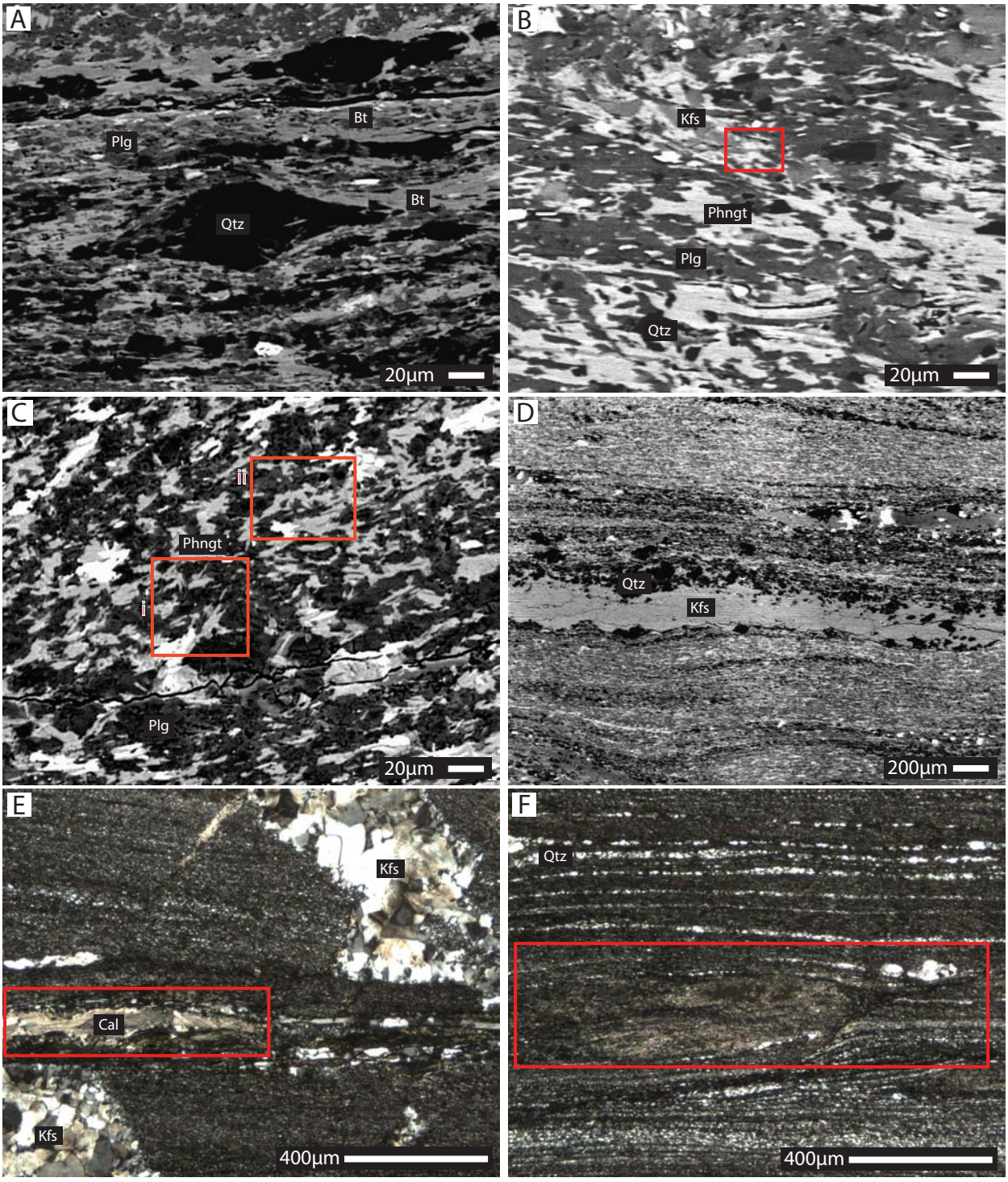
A
Bt
Plg
Bt
Qtz
20µm
B
Kfs
Phngt
Plg
Qtz
20µm
C
ii
Phngt
i
Plg
20µm
D
Qtz
Kfs
200µm
E
Kfs
Cal
Kfs
400µm
F
Qtz
400µm

Figure 8

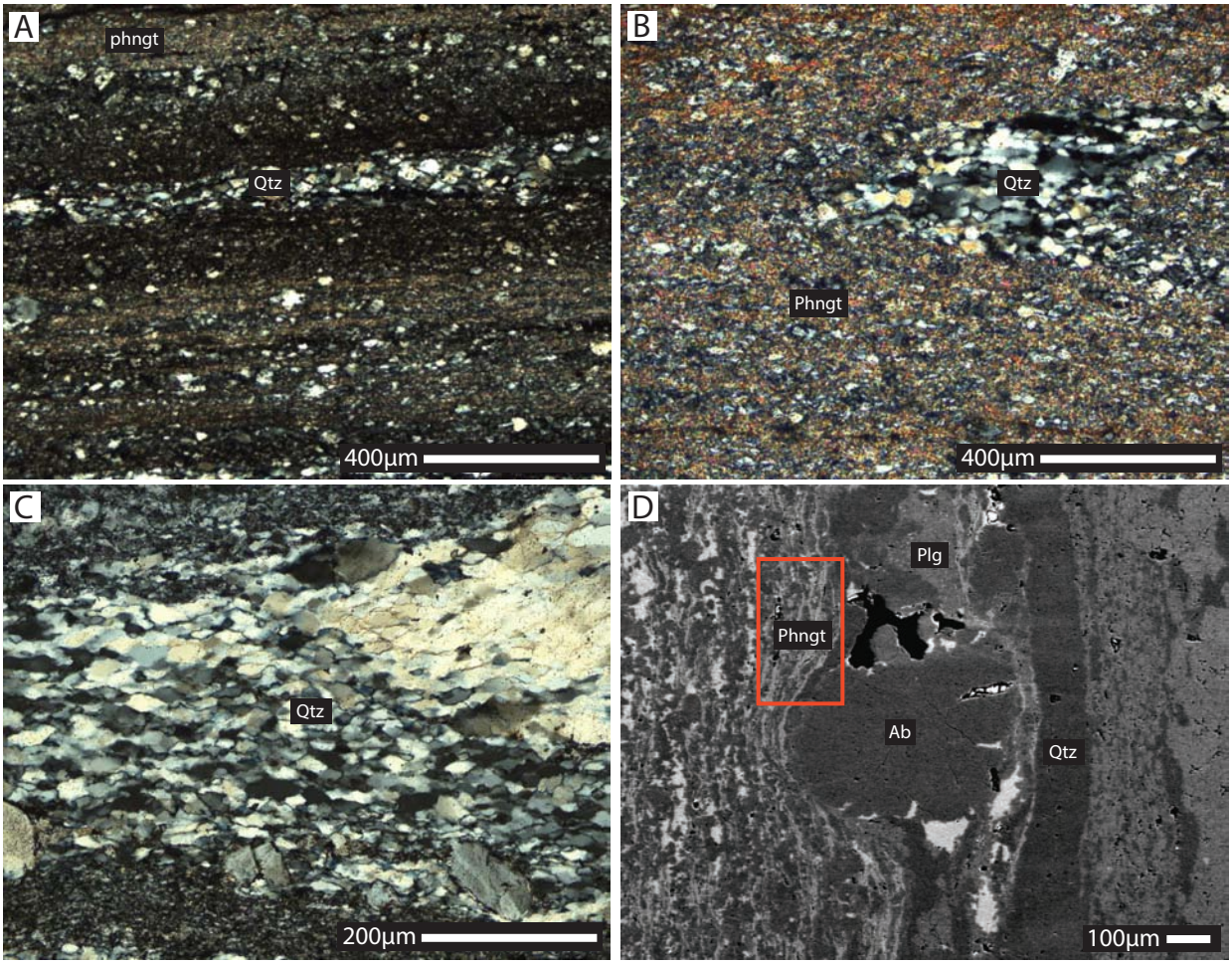
A
phngt
Qtz
400µm
B
Qtz
Phngt
400µm
C
Qtz
200µm
D
Plg
Phngt
Ab
Qtz
100µm

Figure 9

Appendix

Station	UTM Coordinates (NAD27)	Lithology
1	0586883 E 4996805 N	Mylonitic FRF
2	0587021 E 4997023 N	Mylonitic FRF
3	0586850 E 4997127 N	Mylonitic FRF
4	0586664 E 4996974 N	Mylonitic FRF
5	0584456 E 4996143 N	Foliated FRF
6	0585774 E 4997258 N	Foliated FRF
7	0586191 E 4996790 N	Mylonitic FRF
8	0586217 E 4996757 N	Mylonitic FRF
9	0586629 E 4996727 N	Mylonitic FRF
10	0586371 E 4996953 N	Mylonitic FRF
11	0587275 E 4996968 N	Mylonitic FRF
12	No coordinates	Traverse through woods, trying to get to water faster than by canoe, no outcrops
13	0586668 E 4996987 N	Mylonitic FRF
14	0586765 E 4997077 N	Mylonitic FRF
15	No coordinates	Traverse in search of transition zone, no outcrop found, glacial till cover
16	No coordinates	Traverse in search of transition zone, no outcrop found, glacial till cover
17	No coordinates	Traverse in search of transition zone, no outcrop found, glacial till

		cover
18	0590172 E 4996884 N	Breccia in float, thought to be placed
19	0588748 E 4997877 N	Transition between foliated and mylonitic FRF
20	0588584 E 4997780 N	Transition between foliated and mylonitic FRF
21	0589205 E 4997590 N	Granite with small shear zones
22	0587153 E 4997138 N	Mylonitic FRF
23	No coordinates	Traverse in search of transition zone, no outcrop found, glacial till cover
24	No coordinates	Traverse in search of transition zone, no outcrop found, glacial till cover
25	No coordinates	Traverse in search of transition zone, no outcrop found, glacial till cover
26	No coordinates	Baked contact of FRF and granite
27	0587095 E 4996901 N	Mylonitic FRF